D-SCOPE: Diffusion-based Sonar Counterfactual and Prototype Explanations

Anonymous authors
Paper under double-blind review

Abstract

The harsh conditions of underwater environments pose significant challenges for effective monitoring. While using cameras is possible, they are typically limited to short ranges due to underwater visibility conditions. SOund NAvigation and Ranging (SONAR) can perceive objects at greater distances, but produces low-visibility images that are hard to interpret, even for experts. When Artificial Intelligence (AI) methods are used on these SONAR images, Explainable Artificial Intelligence (XAI) methods might help the user understand the AI outputs. Traditional explainability methods, such as saliency maps or perturbation-based visualisations, often struggle to provide informative explanations when applied to low-contrast imagery. This work introduces Diffusion-based SONAR COunterfactual & Prototype Explanations (D-SCOPE), a novel post-hoc explainability framework for SONAR image classification. Our presented approach leverages classifier-guided diffusion models, trained on two publicly available Marine Debris Forward-Looking SONAR datasets, to generate two types of visual explanations: (1) counterfactual explanations that highlight minimal semantic changes to alter a model's decision, and (2) prototype-based explanations for case-based reasoning that translate representative RGB samples into the SONAR domain, serving as intuitive visual references. For counterfactual explanations, a semi-factual explanation is generated by displaying the intermediate steps leading to a change in prediction. For the prototype-based explanation, class-specific prototypes are provided. To the best of our knowledge, this is the first approach applying diffusion-based generative models for explainability in the SONAR modality. Guided diffusion models are shown to produce high-fidelity, class-conditioned counterfactuals in challenging underwater settings. In addition, the proposed cross-domain prototype generation mechanism enhances human interpretability by bridging the gap between clear and recognisable RGB representations and SONAR imagery. Our framework is validated through qualitative and quantitative experiments as well as a controlled human evaluation. The code and the pretrained models shall be released to support further research.

1 Introduction

SONAR sensors play a critical role in underwater scene understanding, particularly in applications such as marine habitat monitoring, Search & Recovery (SAR), and lake surveillance (Elsayed et al., 2024). However, their outputs are often difficult to interpret, making it challenging for humans to trust deep learning systems deployed in such environments. While recent advances in underwater object recognition using deep learning have shown promising results (Wen et al., 2024; Aubard et al., 2024; Li et al., 2024; Zhang et al., 2022), these models are commonly considered as black-box models. This can raise important concerns: how do we make these models more trustworthy for end-users or provide meaningful feedback to developers when they fail? The field of XAI addresses these concerns, and it is growing particularly in high-stakes domains such as healthcare (Band et al., 2023) and autonomous driving (Atakishiyev et al., 2024), where model explainability is crucial. Research has just started to explore XAI in the context of SONAR imagery (El-Mihoub et al., 2024; Natarajan & Nambiar, 2024), yet there remains a significant gap in providing visual explanations for classification and detection results.

Nowadays, generative models, such as Generative Adversarial Networks (GANs) and diffusion models, demonstrate their ability to produce realistic images that are hard to distinguish from real data (Li et al., 2025). These capabilities enable new types of visual explanations, e.g., counterfactuals (Van Looveren et al., 2021; Jeanneret et al., 2022). A Counterfactual Explanation (CE) answers a "what-if" question:" What if this feature had a different value? Would the outcome of the model change?" However, depending on the context, CE can address broader questions (Verma et al., 2020). For example, in terms of causality, CE addresses the question "which features caused this outcome?" Answering this question can be done by identifying minimal changes needed to change the models' outcome. From an actionability perspective, it addresses the question, "which features should be modified to reach a desired outcome?" as in the case of loan approval scenarios. From a contrastive perspective, it can answer the question "why is this outcome produced by the model instead of another?" by comparing factual and counterfactual instances. Beyond counterfactuals, generative models can also support Case-Based Reasoning (CBR) through Prototype-based Explanation (PE) (Li et al., 2018). A prototype serves as a representative or "typical" example of a class, helping users understand what the model considers as characteristic input patterns. Synthesising such prototypes provides an intuitive, concept-level understanding that complements instance-level counterfactual reasoning.

In this work, we introduce D-SCOPE, a post-hoc explainability framework that provides two main visual explanation methods: (1) CEs that shows how an input could be modified to change a prediction, and (2) PEs that illustrates what a typical input of a predicted class looks like. For the CEs, a query image and a user-defined target class are provided. The framework then generates a modified version of the query image classified as the target, along with Semi-factual Explanation (SE), a sequence of intermediate images showing the gradual semantic changes leading to the prediction shift. A pixel-wise difference map is also produced to highlight the regions responsible for the decision change. For the PEs, we generate class-specific prototypes by translating known examples from one modality (e.g., RGB) into another (e.g., SONAR). These synthetic images serve as cross-domain visual references that help users interpret the classification results by comparing them with a typical and semantically grounded example. Unlike saliency-based techniques that only localise attention, this method offers recognisable object appearances that reflect how the model perceives each class. To the best of the authors' knowledge, this is the first work to explore visual CEs and PEs using diffusion models in the context of SONAR imagery. Our main contributions are:

1. D-SCOPE, a unified post-hoc explainability framework for black-box classifiers in underwater SONAR imagery, leveraging generative diffusion models.
2. An empirical demonstration of guided diffusion models for generating class-conditioned counterfactuals in noisy, grayscale SONAR images.
3. A prototype-based explanation strategy for CBR, where a single guided diffusion model performs cross-domain translation (e.g., RGB to SONAR) to generate class-representative examples.
4. Qualitative, quantitative, and controlled human evaluations of the proposed D-SCOPE framework.

The rest of the paper is organised as follows: Section 2 discusses related work. Section 3 reviews the diffusion model concepts and presents our proposed methodology. Section 4 covers the experimental evaluation. Finally, Section 5 concludes with a summary and future directions.

2 Related Work

XAI (Gunning et al., 2019; Atzmueller et al., 2024) methods are crucial for improving the transparency and trustworthiness of deep learning black-box models. Yet, XAI addresses different user types, ranging from non-experts to domain specialists (Ford & Keane, 2022) and can be either intrinsic (through interpretable model design) (Atzmueller et al., 2024) or post-hoc (after model prediction) (Nolle et al., 2023). In this paper, we focus specifically on post-hoc explainability for classification models.

2.1 Post-hoc Explanation Methods

Below, we outline major categories of explanation methods for our application context.

Feature Attribution Methods, such as feature importance or local perturbations, are both post-hoc methods used to explain classification decisions (Ribeiro et al., 2016; Lundberg & Lee, 2017). While these methods might be useful in domains where the images are naturally interpretable by human eyes, these approaches are less effective for perceptual data like SONAR images. In SONAR, pixel-level attributions can still be uninterpretable for human eyes, especially when the images are characterised by low resolution and significant acoustic shadowing.

Prototype-based Explanations (PE) show examples (prototypes) that are representative of the predicted class. This method bridges the human way of thinking, addressing the statement that *"this image is identified as that class, because this image (or part of it) contains something similar to a prototype image (or part of it) that I know."* By providing such examples, the model offers an intuitive explanation to AI users, helping them to understand the decision-making process (Chen et al., 2019; Nauta et al., 2021; Rymarczyk et al., 2022; Schlinge et al., 2025).

Counterfactual Explanations (CE) address potential "what-if" scenarios by identifying a minimal change required to alter a model's prediction. This provides model-agnostic insights without inspecting the internal structure of the model (Wachter et al., 2017). In other words, visual CEs aim to explain a classification through minimal changes in the input image to cross the decision boundary of the classifier, while remaining interpretable to the end-users (Goyal et al., 2019).

Semi-factual Explanations (SE) address "even-if" scenarios that change the input image, but the classifier has to yield the same result as before (Kenny & Keane, 2021). While less commonly used, they complement CEs by showing the prediction invariance.

2.2 Generative Models for Counterfactuals

Generative Models such as GANs (Goodfellow et al., 2014) and diffusion models (Sohl-Dickstein et al., 2015) have been used to produce synthetic data that resembles real data. They have been used in image generation tasks, image editing, and semantic segmentation (Croitoru et al., 2023). In particular, GANs (Goodfellow et al., 2014) learn to generate realistic samples via adversarial training, but suffer from issues such as mode collapse and instability (Chen, 2021). Diffusion models, inspired by non-equilibrium thermodynamics, represent a newer class of generative models. They work by progressively adding noise to data and then learning to reconstruct it, enabling the generation of high-fidelity images (Sohl-Dickstein et al., 2015). Diffusion models are easier to train and more stable than GANs, although they suffer from problems such as bias amplification in the training dataset (Yang et al., 2023).

Counterfactuals produced by Generative Models have been used to produce CE by learning a manifold of realistic variations. They can generate samples that lie between a real image and the region where the classifier would predict a different class, creating a synthetic image that is close to another class but still shares some traits with the original. Several works have used GANs to generate CE in domains such as autonomous driving (Zemni et al., 2023), medical imaging (Mertes et al., 2022), and facial attributes manipulation (Van Looveren et al., 2021). Some of these have included human-centred evaluations, showing that such CE examples can be more effective than state-of-the-art saliency-based explanation methods (Mertes et al., 2022; Zemni et al., 2023).

More recently, diffusion models have been explored for CE generation due to their improved stability and image quality. This includes both unconditional (Jeanneret et al., 2022) and conditional (Favero et al., 2025; Kim et al., 2024; Varshney et al., 2025) diffusion approaches. These works show that diffusion-based counterfactuals are high-fidelity, realistic, and semantically consistent.

2.3 Explainability in SONAR Imagery

XAI for sonar-based AI models is still relatively underexplored. Most existing methods rely on visualisations, e.g., saliency maps or self-attention, applied to classification (Natarajan & Nambiar, 2024) or detection (El-Mihoub et al., 2024; Manss & El-Mihoub, 2025). These are often not reliable, especially when the images are noisy or visually hard to interpret. Perturbation-based explanation methods have been used to investigate the factors influencing the performance of fine-tuned models on Synthetic Aperture Sonar (SAS) data (Walker et al., 2021). Other similar methods, such as submodular approaches to local explanation, have also been applied to interpret deep learning models for underwater sonar image classification (Natarajan & Nambiar, 2024). Saliency maps have been employed to explain the classification of SAS images by convolutional neural networks (CNNs). However, evaluations have shown that end-users remain unconvinced about the effectiveness of these methods (Richard et al., 2024).

SONAR images represent acoustic backscatter intensity patterns; while they may appear visually similar to optical images, they belong to a different modality compared to RGB images. Recent works have explored translating between modalities, such as from SONAR to RGB, to improve human monitoring in low-visibility environments (Wehbe et al., 2022). While these GAN-based approaches enhance the visual interpretability of the scene for a human observer, they do not provide insights into the decision-making process of a classifier. In contrast, PEs and CEs generated via diffusion models offer a new direction by providing user-centred explanations that highlight the features driving a specific classification outcome.

3 Post-hoc Explainability Framework

We propose D-SCOPE, a post-hoc explainability framework for interpreting the predictions of SONAR-based classifiers. The framework does not require access to the internal structure or parameters of the model. It relies on a class-conditional diffusion model and is guided by a classifier trained on images with added Gaussian noise to generate visual explanations. These include counterfactual images that show how an object would appear if it belonged to a different class, along with the intermediate images generated before the prediction changes, which we refer to as SE. In addition, the framework supports prototype-based explanations that map optical-domain examples into their SONAR equivalents. Our framework works with classifiers and detectors trained on the Marine Debris Forward-Looking SONAR dataset (Valdenegro-Toro et al., 2025).

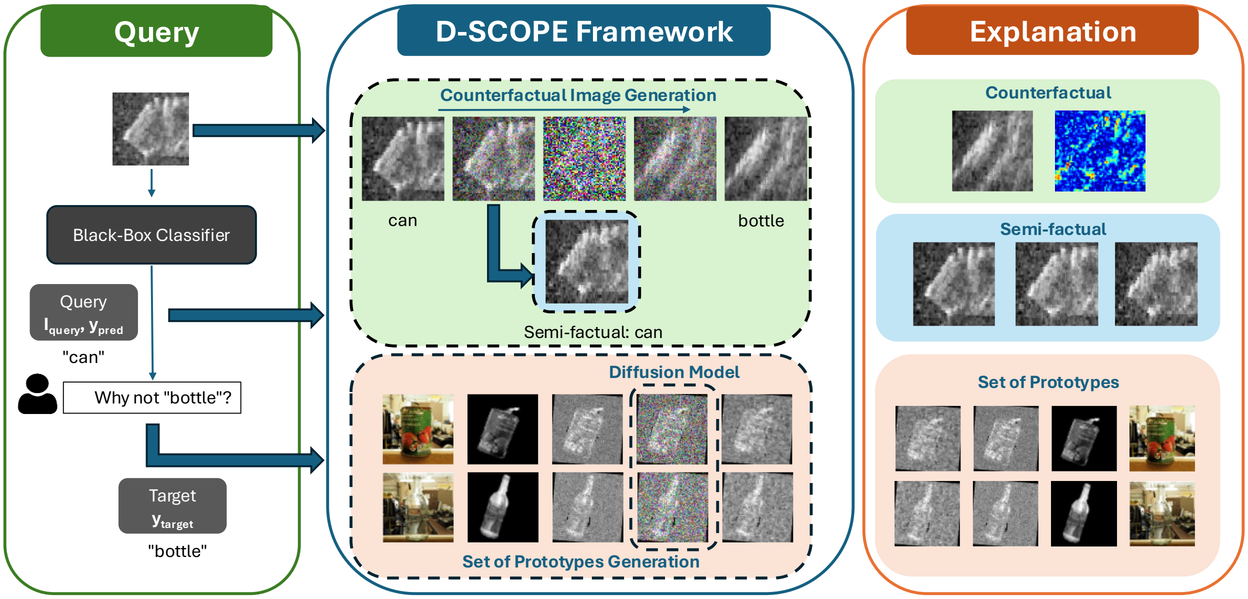

Figure 1: Overview of the explainability framework D-SCOPE for SONAR imagery.

Figure 1 illustrates the proposed framework. The respective steps of the D-SCOPE explanation pipeline are as follows:

1. Consider a SONAR image $\mathbf{X} \in \mathbb{R}^{h \times w}$, with $h, w \in \mathbb{N}$, and a classifier C. Then, a class prediction y_{pred} is generated by $C(\mathbf{X}) = y_{\text{pred}}$.
2. The user then asks questions about the classification, such as: *"Why is this not classified as y_{target}?"*
3. Accordingly, the target class y_{target}, along with $\mathbf{X}$, is forwarded to the explanation module, i.e. the guided diffusion model.
4. After that, the user chooses the type of explanation:
   - **Counterfactual Explanation:** A class-conditional diffusion model generates a counterfactual image $\widehat{\mathbf{X}}_{\text{cf}}$ aligned with y_{target}.
   - **Prototype-based Explanation:** The diffusion model performs cross-domain translation (e.g., from optical to SONAR) to generate prototype images. Then, $\widehat{\mathbf{X}}_{\text{pred}}$ is a prototype for y_{pred} and $\widehat{\mathbf{X}}_{\text{target}}$ is a prototype for y_{target} in a familiar modality, e.g., RGB.
5. Next, the generated image (either $\widehat{\mathbf{X}}_{\text{cf}}$, $\widehat{\mathbf{X}}_{\text{pred}}$, or $\widehat{\mathbf{X}}_{\text{target}}$) is presented to the user, who may request refinement or explore additional target classes or explanation modes.

3.1 Diffusion Models

Diffusion models iteratively add noise to an image and then learn how to remove the noise. To achieve this, diffusion models treat the input image as a random variable such that it can be modelled by a distribution, i.e. $\mathbf{X} \sim q(\mathbf{X})$. Then, a forward Markov process is defined to add noise to the input image. The resulting noisy image can then be defined as (Nichol & Dhariwal, 2021):

$$q(\mathbf{X}_1, \ldots, \mathbf{X}_T \mid \mathbf{X}) = \prod_{t=1}^{T} q(\mathbf{X}_t \mid \mathbf{X}_{t-1}) = \mathcal{N}\Big(\mathbf{X}_t; \sqrt{1-\beta_t}\mathbf{X}_{t-1}, \beta_t \mathbf{I}\Big) \tag{1}$$

where $\mathbf{X}_t$ is the noisy image at timestep $t = 1, \ldots, T$, $\beta_t \in (0, 1)$ controls the noise added at each step, and $\mathbf{I}$ is the identity matrix. Accordingly, this notation might yield $\mathbf{X}_0$, which is equal to $\mathbf{X}$.

This process is reversible (Ho et al., 2020) and is modelled by a neural network that approximates the reverse transitions

$$p_\theta(\mathbf{X}_{t-1}|\mathbf{X}_t) \quad = \quad \mathcal{N}(\mathbf{X}_{t-1}; \mu_\theta(\mathbf{X}_t, t), \Sigma_\theta(\mathbf{X}_t, t)), \tag{2}$$

where θ denotes the model parameters, $\mu_\theta(\mathbf{X}_t, t)$ is the predicted mean, and $\Sigma_\theta(\mathbf{X}_t, t)$ is the predicted variance at timestep t.

In the forward process, the image is gradually transformed into noise, such that $\mathbf{X}_T \sim \mathcal{N}(0, \mathbf{I})$. The reverse process then iteratively maps noise back to the data distribution (Nichol & Dhariwal, 2021).

To guide the generation toward a specific object class in SONAR imagery, we use a class-conditional diffusion model, where the network is conditioned on the target class y_{target}. Building on the works of (Dhariwal & Nichol, 2021), this enables the generation of counterfactuals and prototypes that illustrate how an object might appear if it belonged to a different class. The denoising process is learned through a neural network, which we refer to as the diffusion model $\mathcal{D}_\theta$. This network predicts the mean and variance in the reverse process $p_\theta(\mathbf{X}_{t-1}|\mathbf{X}_t)$, as in equation 2.

3.2 Counterfactual Explanations (CE) & Semi-Factual Explanations (SE)

When the user requests a CE for a black-box classifier's prediction, the framework generates a CE by perturbing the input image $\mathbf{X}$ with its predicted label y_{pred}. Noise is added to $\mathbf{X}$ to produce a noisy sample $\mathbf{X}_t$ at timestep $t \in \{1, \ldots, S\}$, where $S = 160$. This uses time respacing (Nichol & Dhariwal, 2021) to reduce the inference schedule for better computational efficiency. The noise is then removed through a reverse diffusion process guided by a class-conditional diffusion model $\mathcal{D}_\theta$. At each denoising step, the noisy classifier $\mathcal{C}_{\text{noisy}}$ provides the log-probability of the target class, $\log p_{\mathcal{C}_{\text{noisy}}}(y_{\text{target}}|\mathbf{X}_i)$, and its gradient $\nabla \mathbf{X}_i$ is used to perturb the sample toward the target class (Classifier Guidance). This produces a sequence of intermediate denoised samples $\mathbf{X}_i$, illustrating the gradual transformation from the query class toward the target class.

A candidate sample is recorded as valid if both classifiers predict the target class above a confidence threshold τ. The framework selects the best counterfactual $\mathbf{X}_{\text{cf}}$ (usually corresponding to the minimal timestep that flips the prediction). It computes a pixel-wise difference map $\Delta = |\mathbf{X} - \mathbf{X}_{\text{cf}}|$ and SSIM score to quantify structural similarity to the original image.

With a fixed time respacing, the added noise to the input image is the only parameter that is changed gradually, aiming for a classifier that gives a prediction above a certain threshold. If the target class y_{target} is reached, the loop breaks, and a counterfactual is generated along with a pixel-wise difference map that shows what has been changed. We compute Structural Similarity Index Measure (SSIM) scores between the query SONAR image and its counterfactual generated SONAR image to show the user how much the query image needs to be modified to produce a counterfactual image. SSIM captures low-level structural differences and provides an intuitive measure of visual shifts (see Section 4.3). The counterfactual generation method is described in Algorithm 1.

Algorithm 1 Counterfactual Generation via Guided Diffusion

```
Require: Query image $\mathbf{X}$, target class $y_{\text{target}}$, diffusion model $\mathcal{D}_\theta$, noisy classifier $\mathcal{C}_{\text{noisy}}$, classifier $\mathcal{C}$, guidance weight $\lambda$, confidence threshold $\tau$, max steps $S = 160$
Binary search for minimal timestep $t^* \in \{1, \dots, S\}$
while binary search has not converged do                ▷ Search for minimal noise level
    Select candidate timestep $t$
    Add noise to $\mathbf{X}$ at timestep $t$
    for $i = t$ down to 1 do                             ▷ Denoising loop
        Predict mean $\mu_i$ using $\mathcal{D}_\theta(y_{\text{target}})$
        Compute gradient $\mathbf{g} \leftarrow \nabla_{\mathbf{X}_i} \log p_{\mathcal{C}_{\text{noisy}}}(y_{\text{target}}|\mathbf{X}_i)$
        Apply guidance: $\mu_i \leftarrow \mu_i + \lambda\sigma_i^2\mathbf{g}$
        Sample $\mathbf{X}_{i-1} \sim \mathcal{N}(\mu_i, \sigma_i^2)$
    end for
    Candidate $\mathbf{X}_{\text{cf}}^{(t)} \leftarrow \mathbf{X}_0$
    if $\mathcal{C}(\mathbf{X}_{\text{cf}}^{(t)}) \geq \tau$ and $\mathcal{C}_{\text{noisy}}(\mathbf{X}_{\text{cf}}^{(t)}) \geq \tau$ then
        Record candidate $\mathbf{X}_{\text{cf}}^{(t)}$ as valid; adjust search for smaller $t$
    else
        Adjust search for larger $t$
    end if
end while
Select best counterfactual $\mathbf{X}_{\text{cf}}$ associated with $t^*$
Compute $\Delta = |\mathbf{X} - \mathbf{X}_{\text{cf}}|$, SSIM return $\mathbf{X}_{\text{cf}}, \Delta$, SSIM
```

Our approach employs a class-conditional diffusion model, which directly conditions on the target class during generation. Unlike unconditional models that rely on classifier guidance during sampling, this allows more precise control over the generated images and produces counterfactuals that are well-suited for interpreting SONAR imagery.

To provide context for the generated counterfactuals, each SONAR class is annotated with its material (e.g., metal, plastic, composite, rubber) and general shape (e.g., cylindrical, rectangular, toroidal, linear, complex). This information is made available to the user through plots and visualisations, giving an intuitive understanding of the respective object properties. By referencing these attributes, users can better interpret the plausibility of the counterfactual images and understand how structural or material changes relate to the original query.

3.3 Prototype-based Explanations (PE)

In addition to CE, D-SCOPE framework supports PE. We utilise the Image-to-Image translation (I2I) concept to convert an object from the optical domain to the SONAR domain using a conditional diffusion model (Saharia et al., 2022). Instead of relying on latent vectors or image patches to justify class predictions (Chen et al., 2019), we generate cross-modal prototypes using our trained conditional diffusion model. These images serve as prototypes of what objects in a given class would look like in the other modality. These prototypes help humans interpret the SONAR outputs in familiar visual ways (e.g., Optical RGB images) and understand what the objects would have looked like from a SONAR perspective. In other words, we can say this PE within D-SCOPE framework makes the human think: "This looks like an example that I know" (as in the optical domain).

The user asks why the classifier identifies an object in a SONAR image as, for example, a *valve* (see Figure 2. We start from predefined RGB prototypes in the dataset and select the corresponding object image. The object's background is removed, and the cropped region is converted to greyscale. We then apply Contrast Limited Adaptive Histogram Equalization (CLAHE) (Pizer et al., 1987) with added noise to match the contrast characteristics of the target SONAR image. The noise added is zero-mean Gaussian noise ($\mathcal{N}(0, 0.05)$), to resemble more the SONAR characteristics and stabilise the diffusion input.

As illustrated in Algorithm 2, the process of prototype-based explanations is iterative. A predefined RGB prototype image corresponding to the target class is first converted into a background-removed greyscale image, after which augmentations (flipping, stretching, zooming) are applied. The augmented image is then passed through the diffusion model with a fixed noise level $t = 30$ (within the $T = 160$ respaced schedule) and a classifier scale set to 1.0. At this noise level, the model has sufficient denoising steps to bridge the domain gap between the RGB prototype image and realistic sonar acoustic appearance, while preserving its underlying geometry. To guide this process towards a representative explanation, we propose a multi-objective loss function (Equation 3). This function evaluates the generated prototype against two reference targets: (i) the target SONAR image, with a focus on matching orientation using cosine similarity while also discouraging deviations in visual style, and (ii) the preprocessed input image (pre-diffusion), which guides visual appearance preservation via SSIM. This feedback loop continues until a prototype is obtained that is interpretable to the user in terms of orientation and visual appearance, as reflected by the loss criteria.

The loss function used to select the best prototype is defined as

$$\begin{aligned}\mathcal{L} = \alpha\left(1 - \mathrm{SSIM}\Big(\mathbf{X}_{\text{processed}}, \widehat{\mathbf{X}}_{\text{proto}}\Big)\right) + \gamma\left(1 - \mathrm{SSIM}\Big(\mathbf{X}_{\text{target}}, \widehat{\mathbf{X}}_{\text{proto}}\Big)\right)\\ + \delta(1 - S_{\cos}(\mathbf{X}_{\text{target}}, \widehat{\mathbf{X}}_{\text{proto}}))\end{aligned} \tag{3}$$

where $S_{\cos}$ denotes the cosine similarity of pixel intensities, and α, γ, and δ are weighting coefficients. The first term enforces structural consistency with the processed RGB prototype adapted to sonar appearance, while the second and third terms encourage similarity between the generated prototype and the target sonar image using SSIM and cosine similarity over pixel intensities, respectively. We empirically set the weights to $\alpha = 0.1, \gamma = 1.0$, and $\delta = 0.2$. This configuration prioritises alignment with the target class characteristics while providing the diffusion model enough flexibility to translate the source geometry into a realistic sonar texture.

4 Experiments & Evaluation

This section presents the experimental setup and evaluation of D-SCOPE framework for generating counterfactual and prototype explanations using diffusion models on sonar imagery. We evaluate both the fidelity of the generated images and the closeness of the explanations to the real images, using quantitative metrics, qualitative case studies, and a user study.

Algorithm 2 Prototype-Based Explanation via Diffusion

```
Require: Target SONAR image $\mathbf{X}_{\text{target}}$, target label $y_{\text{target}}$, RGB prototype set $\mathcal{P}$
Output: SONAR-style prototype $\widehat{\mathbf{X}}_{\text{proto}}$ explaining the classification of $\mathbf{X}_{\text{target}}$ as $y_{\text{target}}$
Select an RGB prototype image $\mathbf{X}_{\text{rgb}} \in \mathcal{P}$ for class $y_{\text{target}}$
Remove background from $\mathbf{X}_{\text{rgb}}$ and convert to greyscale $\mathbf{X}_{\text{grey}}$
Apply random augmentation (e.g., flip, scale, shift)
Apply CLAHE and add Gaussian noise $\mathcal{N}(0, 0.05)$, obtaining $\mathbf{X}_{\text{processed}}$
Set diffusion parameters: classifier scale = 1.0, noise level = 30
repeat
    Add noise to $\mathbf{X}_{\text{processed}}$ at timestep $t$: $\mathbf{X}_t \leftarrow q(\mathbf{X}_t|\mathbf{X}_{t-1})$
    Denoise using diffusion model: $\widehat{\mathbf{X}}_{\text{proto}} \leftarrow p_\theta(\mathbf{X}_{t-1}|\mathbf{X}_t)$
    Compute loss $\mathcal{L}$ as defined in equation 3
until Lowest loss is found or max iterations reached
return $\widehat{\mathbf{X}}_{\text{proto}}$                                        ▷ Best candidate
```

4.1 Experimental Setup

Datasets:

We utilised the *Watertank* and *Turntable* datasets (Singh & Valdenegro-Toro, 2021; Valdenegro-Toro et al., 2025), both acquired under controlled SONAR conditions. From the *Watertank* dataset, we selected 8 of the original 10 classes: **bottle**, **can**, **chain**, **drink carton**, **hook**, **propeller**, **tire**, and **valve**. From the *Turntable* dataset, we selected 9 of 12 classes: **bidon**, **bottle**, **box**, **can**, **drink-carton**, **pipe**, **tire**, **valve**, and **wrench**.

We excluded some classes from both datasets due to low visual plausibility for explanations, insufficient class diversity, and/or strong background dependence. Overlapping classes across datasets (e.g., plastic-pipe) were treated as distinct due to differences in acquisition conditions. The remaining classes nonetheless include challenging cases, as shown in Figure 2, where low Signal-to-Noise Ratio (SNR) conditions degrade object structure and class-relevant semantics. This makes training on such data challenging and increases the likelihood that low SNR samples are perceived as implausible when presented as counterfactual or prototype explanations.

All images were resized to 64 × 64 and normalised using standard PyTorch transforms.

Models Configuration: We adopted the public diffusion model codebase from (Dhariwal & Nichol, 2021). Table 1 summarises the configuration used for model training. For inference, we use timestep respacing with 160 steps; this allows the model to be significantly faster during generation. Instead of sampling at the 2000 steps used during training, we utilise a strided schedule to reduce inference time while maintaining sample quality.

Table 1: Diffusion Model Training Parameters

Model	Image Size: 64	Channels: 128	Residual Blocks: 3
Diffusion	Steps: 2000	Schedule: Cosine	Class Condition: True
Training	Learning Rate: 10^{-4}	Batch: 128	Weight Decay 0.05

Training was performed on an Nvidia RTX 3090 GPU (24GB) for approximately 24 hours. Sampling was later conducted using a lower-memory Nvidia RTX A2000 (4GB) GPU.

Computational Latency: D-SCOPE is an offline XAI tool, not intended for real-time use. On a consumer-grade laptop GPU (e.g., RTX A2000), generating a counterfactual takes 40s–80s depending on the query-target mapping; for example, bottle-to-can is typically faster than valve-to-propeller. Prototype generation is quicker, taking about 16s–28s.

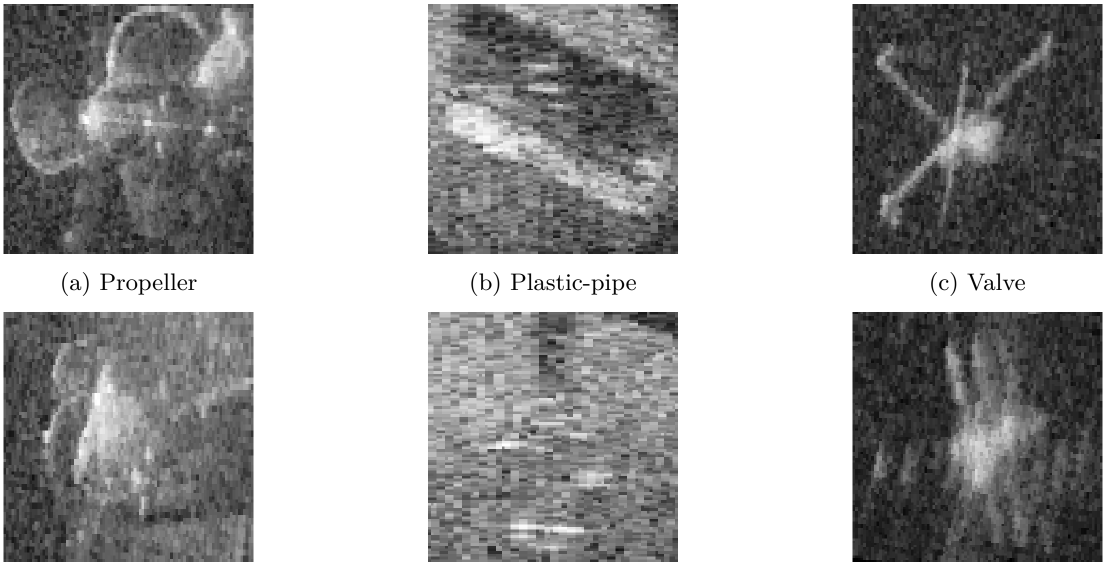

(a) Propeller

(b) Plastic-pipe

(c) Valve

(d) Propeller

(e) Plastic-pipe

(f) Valve

Figure 2: Examples from the Watertank and Turntable datasets. (Top row): High-SNR images with distinct object geometry. (Bottom row): Low-SNR images dominated by speckle noise.

4.2 Classifier Setup

To support guided diffusion and explanation generation, we trained two types of classifiers: standard classifiers on clean SONAR images and noisy classifiers on noise-corrupted images. These were tuned with Optuna (Akiba et al., 2019) and tracked with MLflow (Zaharia et al., 2018).

Classifiers under study We selected two architectures based on their performance and stability during training. For the *Watertank* dataset, we used a **ResNet-18**, which achieved a test accuracy of 96.49%. For the more challenging *Turntable* dataset, we utilised a **DenseNet-121**, reaching a test accuracy of 97.62%. Watertank classes exhibit greater geometric distinctiveness, while Turntable classes show realistic confusion patterns (e.g., "bidon" vs. "bottle") due to visual similarity in sonar imagery. These results establish the baseline behaviour of the classifiers before analysing their responses to counterfactual perturbations and decision boundary transitions.

Noisy classifier. Following the guided diffusion framework (Dhariwal & Nichol, 2021), we trained UNet-based classifiers on noise-corrupted SONAR images ($t \in [0, 2000]$). Training on these noisy images is necessary for the classifier to provide meaningful gradients during the reverse process towards the target manifold. Since the Turntable dataset is more challenging and contains classes that are visually harder to distinguish, we increased the model capacity from a depth of 2 (128 channels) for Watertank to a depth of 4 (256 channels). Both models use attention-based pooling at resolutions of 32, 16, and 8. These noisy classifiers are used to provide class-conditional gradients that steer the reverse diffusion process toward a target class.

4.3 Evaluation Metrics

We evaluate the quality of generated explanations using a combination of statistical and perceptual metrics:

Fréchet Inception Distance (FID) (Heusel et al., 2017): Assesses realism by comparing statistics between real and generated image distributions using features extracted from a pretrained InceptionV3 network. Lower scores indicate that the generated images are more similar in distribution to the distribution of the real images. We acknowledge that FID values may not fully reflect visual realism in sonar imagery, since InceptionV3 is pre-trained on optical imagery.

SSIM (Wang et al., 2004): Assesses structural similarity at the pixel level by comparing luminance, contrast, and structure between the original and generated images. Higher SSIM values indicate more similar image structures. We focus on SSIM to evaluate counterfactual visual fidelity and do not use Learned Perceptual Image Patch Similarity (LPIPS). Although LPIPS captures fine-grained perceptual differences beyond SSIM, it relies on optical-domain features (AlexNet) that may not fully reflect human perception of sonar images. SSIM provides a consistent and interpretable measure of structural changes, which suffices for assessing the minimal modifications needed to generate counterfactuals.

Precision (Kynkäänniemi et al., 2019): Measures the fidelity of the generated images. It reflects the percentage of fake images that lie within the distribution of real images. High precision means the generated images are more realistic and closer to real samples.

Recall (Kynkäänniemi et al., 2019): Measures the diversity of the generated images by estimating how much of the real image distribution is covered by the generated samples. A high recall indicates that the model can produce a wide range of realistic variations.

4.4 Quantitative Analysis: Diffusion Models

We compare classifier-guided diffusion across different classifier scales (0.5 to 3.0). Table 2 summarises the results for 2000 generated samples, using FID, precision, and recall to evaluate image quality and diversity. As the classifier scale increases, FID scores improve, indicating more realistic image generations. However, precision and recall peak at classifier scale 1.0 and drop at higher values. This suggests that stronger guidance improves visual quality but limits diversity. Therefore, scale 1.0 provides the best balance between image quality and variety, making it a suitable setting for both counterfactual and prototype-based generation tasks.

Table 2: Quantitative Evaluation Metrics for 2000 Samples

Scale	**FID** (↓)	**Precision** (↑)	**Recall** (↑)
0.5	3.0	0.37	0.21
1.0	2.8	**0.39**	**0.31**
2.0	2.6	0.37	0.21
3.0	**2.5**	0.37	0.21

4.5 Counterfactuals Evaluation

4.5.1 Quantitative analysis: Counterfactuals

We use the flip threshold (expressed as a percentage of the maximum diffusion noise) as a quantitative metric for counterfactual evaluation. It measures the minimal noise level required to flip the classifier decision from a query class to a target class. The more noise required, the harder the transformation and the longer the reverse diffusion trajectory. With timestep respacing capped at $T = 160$, we identify the minimal timestep $t^* \in [0, 160]$ at which the classifier decision flips to the target class. This timestep directly quantifies the amount of noise added during the forward diffusion and, equivalently, how much noise the reverse diffusion must remove to reach a valid counterfactual. The values reported for each query–target class mapping are averaged over 10 independent generations, resulting in 560 generations for the "Watertank" dataset and 720 for the "Turntable" dataset.

Figure 3 reports this quantity as a percentage of the maximum noise level. A value of 100% corresponds to denoising from pure Gaussian noise, implying that the generated image has no structural relation to the original query image. Lower percentages indicate that the classifier decision can be flipped while preserving more of the original image structure. The "Watertank" dataset exhibits a mean flip threshold of 62% ($\sigma = 9.8\%$), while the Turntable dataset proves more challenging, with a higher mean of 65.7% ($\sigma = 13.66\%$).

The heatmaps visualise these query–target difficulties. In the "Watertank" dataset, transforming a valve query into other classes consistently requires a higher flip threshold, indicating that valves are structurally

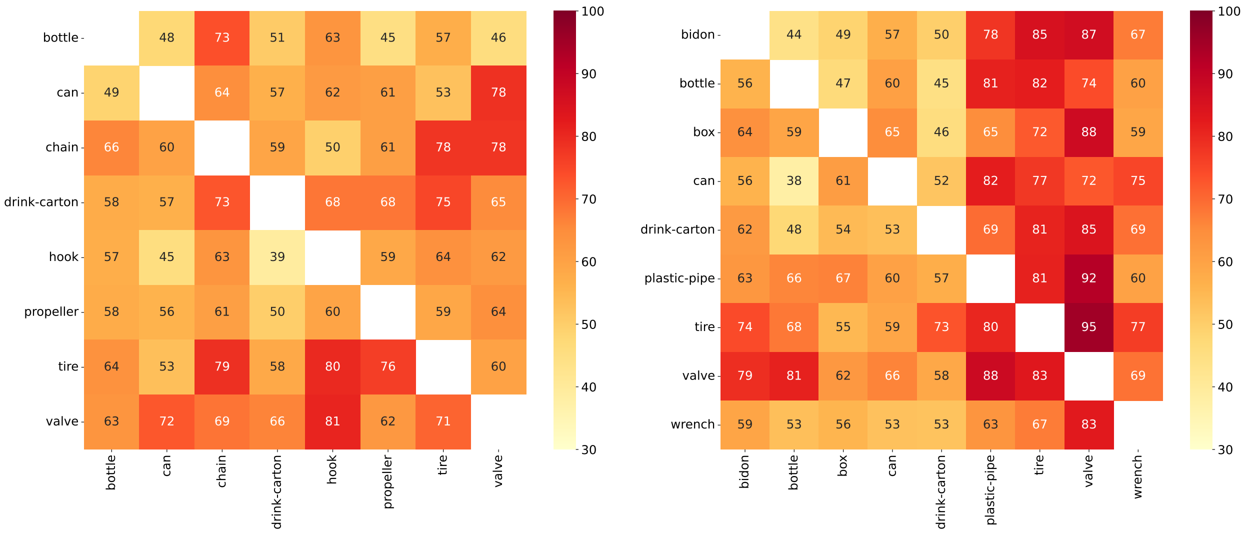

(a) Watertank Dataset

(b) Turntable Dataset

Figure 3: Query–target classifier flip thresholds. Cells show the average minimal noise level % required to flip the classifier.

distinct and harder to modify without destroying their identity. In contrast, flipping a bottle into a valve often requires less noise. This asymmetry arises because, under certain sonar viewpoints, valve returns exhibit elongated shapes that overlap visually with bottles, facilitating boundary crossing (see Figure 2f). Overall, bottle queries are the easiest to transform, indicating that bottle instances are more easily perturbed toward other class decision regions. For the "Turntable" dataset, the most difficult query class is the valve, while the wrench is relatively easier to transform. These results show that classifier decision boundaries can be crossed with substantially less injected noise than would be required to leave the query data manifold.

4.5.2 Qualitative Analysis: Counterfactuals

We analyse the transformations generated from a query image (e.g., user input) into counterfactuals targeting other classes in the two datasets. To assess structural and perceptual changes, we utilise pixel-wise difference maps and SSIM. The difference maps visualise regions of change, highlighting which areas of the image the diffusion model modified to shift the classifier's prediction from the query class to a target class.

Figure 4a presents an example using the class "**can**" as a query in the "Watertank" dataset. The leftmost column shows the original image, followed by seven counterfactuals corresponding to the remaining target classes. Below, each image is accompanied by its corresponding pixel-wise difference map, and the SSIM (per-example) value is listed under it. The lowest score is for the "**propeller**", which can be understandable since that counterfactual involves a significant structural shift, where most of the image is altered to represent a "**propeller**". On the other hand, the **"drink-carton"** has the highest SSIM because it looks quite similar to the original "**can**". However, perceptually, the bottle seems closer to the "can" but it's more out of focus, which results in a lower SSIM score.

For the "Turntable" dataset, Figure 4b shows 8 counterfactual classes against the query class "**can**". The "**bottle**" class is the nearest to the bottle with the highest SSIM compared to other classes, while the "**valve**" has the lowest similarity. For the low SNR sonar images, D-SCOPE can successfully flip the classifier decision to a specified target-class, but the explanation could be less meaningful.

These results reflect the nature of SONAR images: they are often blurry and low in visibility, which can make it difficult to preserve structure when generating convincing counterfactuals for the user. For example, closely-related classes such as "**can**", "**drink-carton**", and **bottle** pose additional challenges. These classes often differ mainly in aspect ratios, making fine-grained changes difficult, and sometimes they can mislead

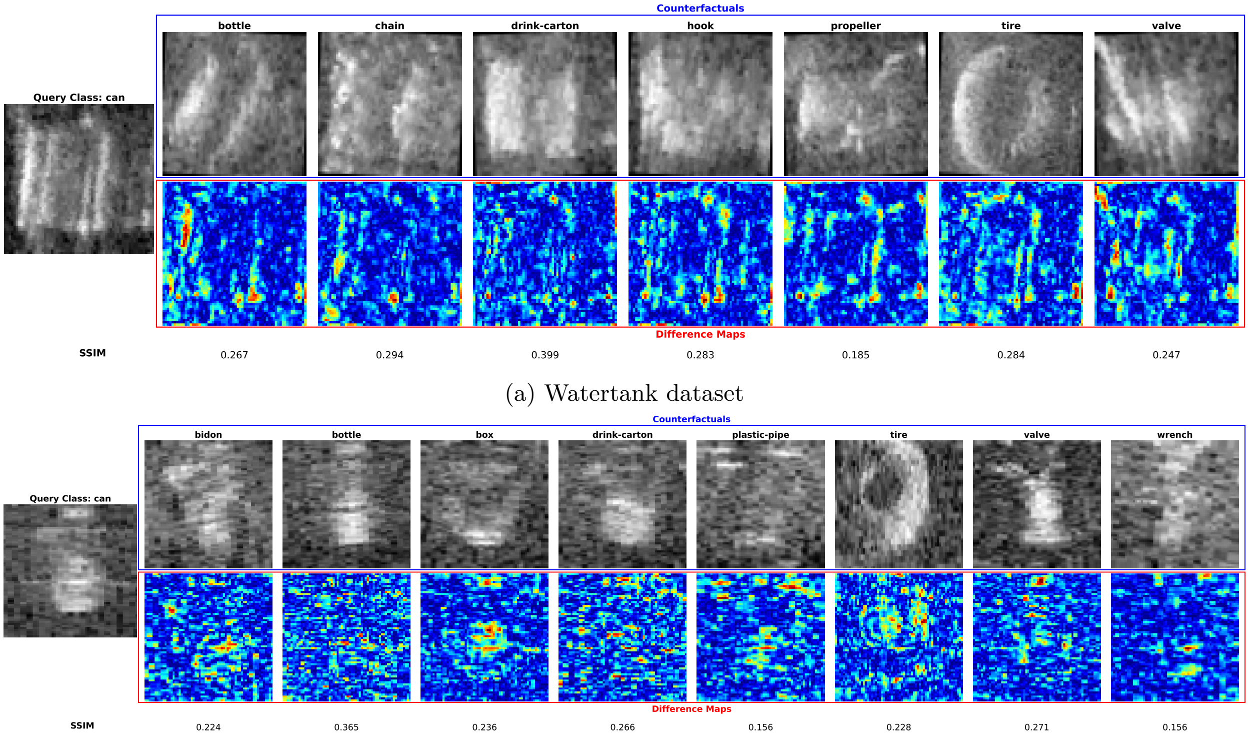

(a) Watertank dataset

(b) Turntable dataset

Figure 4: Query image of class **can** and its counterfactuals (top row) with pixel-wise difference maps (bottom row) and associated SSIM values, for two datasets.

the classifier. Similarly, classes such as "**chain**" and "**hook**" can be problematic, as the "**hook**" class in the dataset often includes a visible chain segment attached to the hook head. This overlap can complicate the procedure of counterfactual generation and interpretation in certain cases. These qualitative examples demonstrate that counterfactuals can provide interpretable insights for SONAR classifiers, even in cases where structural shifts are substantial.

In addition to the final counterfactual, we visualise the intermediate diffusion states preceding the prediction flip, which we refer to as SE. These states form a boundary trajectory that reveals how the input transitions from the query to the target class.

Figure 5 shows representative boundary trajectories for selected query–target pairs from the *Watertank* dataset using a ResNet-18 classifier. Each trajectory consists of successive diffusion states leading up to the first change in predicted label. When time respacing is set to 160 steps, the late stages of the trajectory become increasingly noise-dominated, resulting in a rapid loss of class-specific visual structure.

In Figures 5a and 5b, the classifier flips at timesteps where the generated samples exhibit a clear semantic alignment with the target class (e.g., bottle to valve at timestep 63). In contrast, Figure 5c illustrates a non-monotonic transition: the classifier prediction passes through intermediate classes, such as "hook", before reaching "propeller". This occurs because certain intermediate shapes, such as crescent-like structures, are sufficient to activate the hook decision region despite limited semantic similarity to either endpoint. We nevertheless designate "propeller" as the counterfactual, as it is the first state along the trajectory that achieves the intended query-to-target flip. This example highlights that boundary trajectories need not correspond to smooth or semantically linear transformations.

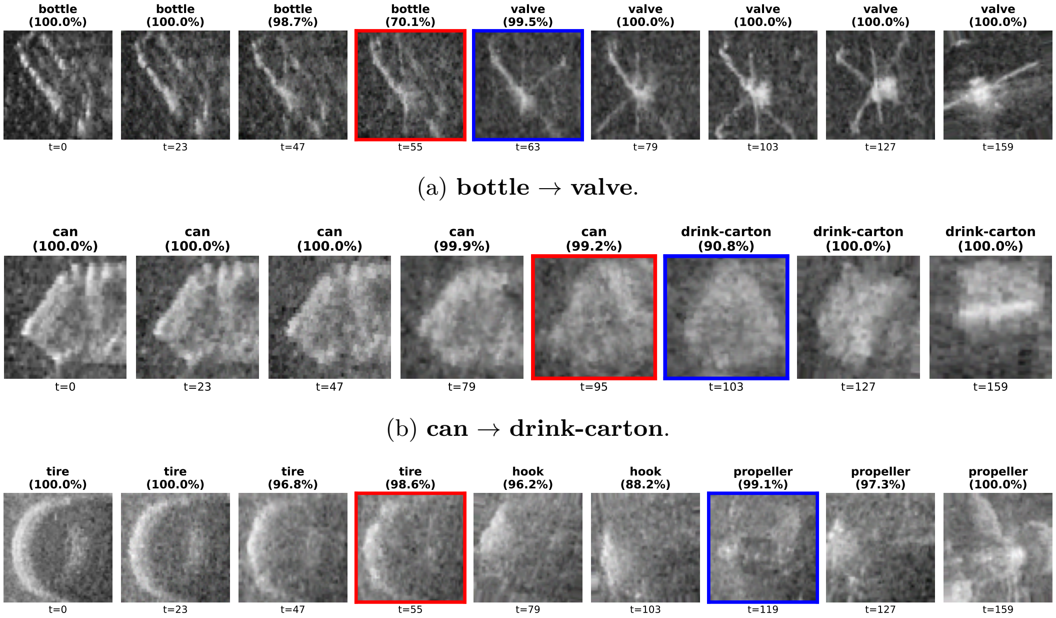

(a) **bottle** → **valve**.

(b) **can** → **drink-carton**.

(c) **tire** → **propeller**.

Figure 5: Boundary trajectories for selected source–target pairs in the *Watertank* dataset using ResNet-18. Semi-factual images are shown in blue and counterfactual images in red.

4.6 Prototypes Evaluation

During prototype generation, we observed that increasing the input noise level in the guided diffusion process led to geometric misalignment between the input and output images. This is because the added noise covers most of the image and tends to override the input geometric structure (orientation). Because our framework lacks explicit spatial conditioning, such as conditioning the diffusion process on segmentation masks, bounding boxes, or ControlNet-style constraints (Zhang et al., 2023). We addressed this challenge by balancing the classifier guidance and the added noise to the input image to try and preserve the geometric alignment to produce semantically meaningful prototypes.

As shown in Figure 6a, the **tire** class demonstrates the most consistent prototype, as its geometry in the input RGB image closely resembles its appearance in the SONAR image. The **valve** is more challenging due to significant viewpoint differences; while the RGB image captures it from the side, the SONAR image represents a top-down perspective. To improve prototype matching for the valve, the RGB input should ideally be captured from a similar top-down view, as perceived by the SONAR. For the **hook**, our algorithm struggled when the RGB input image lacked the structural similarity to the target class in structure. This is when the RGB image only contains the hook head, while the SONAR representation includes both the hook head and an attached chain, leading to mismatched representations.

Figure 6b presents the prototype evaluation for the Turntable dataset. Similar to the Watertank setup, the **tire** class remains one of the easiest. The **valve** shows comparable behaviour across both datasets. More challenging classes include **bidon**, **bottle**, **box**, **can**, **drink carton**, and **plastic pipe**. These objects share similar SONAR appearances, with distinctions primarily arising from aspect ratio rather than shape. This suggests that PE helps bridge semantic understanding between the SONAR and RGB domains, even when object classes are visually ambiguous. The **wrench** class also demonstrates a clear and consistent prototype.

Several failure cases persist, where successful interpretation depends on the existence of a coherent and visually recognisable object structure. When the SONAR image lacks such a structure, as is common in low SNR conditions, the PE fails to establish a meaningful correspondence between the RGB and SONAR

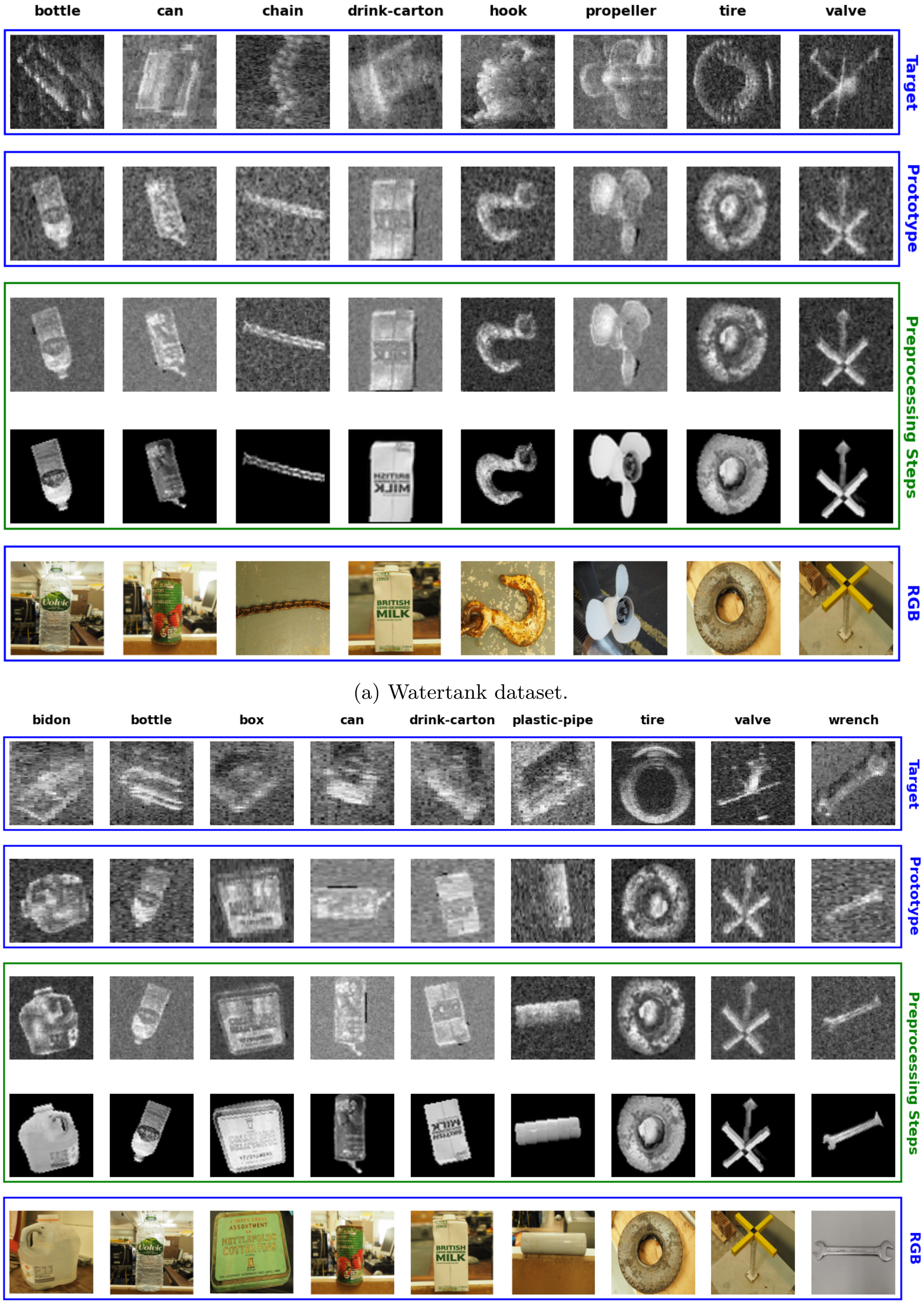

(a) Watertank dataset.

(b) Turntable dataset.

Figure 6: Prototype generation to convert from RGB to SONAR images.

domains. This can be seen in the low SNR samples in Figure 2. Therefore, we treat these cases as dataset-driven limitations and restrict our qualitative analysis to representative cases.

4.7 Evaluation by Humans

To assess the usefulness of our D-SCOPE framework, we conducted a controlled exploratory user study with eight participants of varying machine learning experience levels, giving 128 responses in total. None were sonar domain experts; therefore, the evaluation targets general perceptual interpretability rather than operational validity. Each participant assessed 16 examples sampled equally from the Watertank and Turntable datasets. The study consisted of three sequential phases. First, participants were shown the query image together with the classifier's top two predictions. They rated (i) trust in the classifier and (ii) their ability to recognise semantic structure within the query image. Then, CE or a PE were shown with randomised order. They rated the explanation according to predefined criteria. Lastly, the alternative explanation was revealed and rated in the same manner. Participants then selected which explanation better supported their understanding of classifier behaviour and provided a final trust rating.

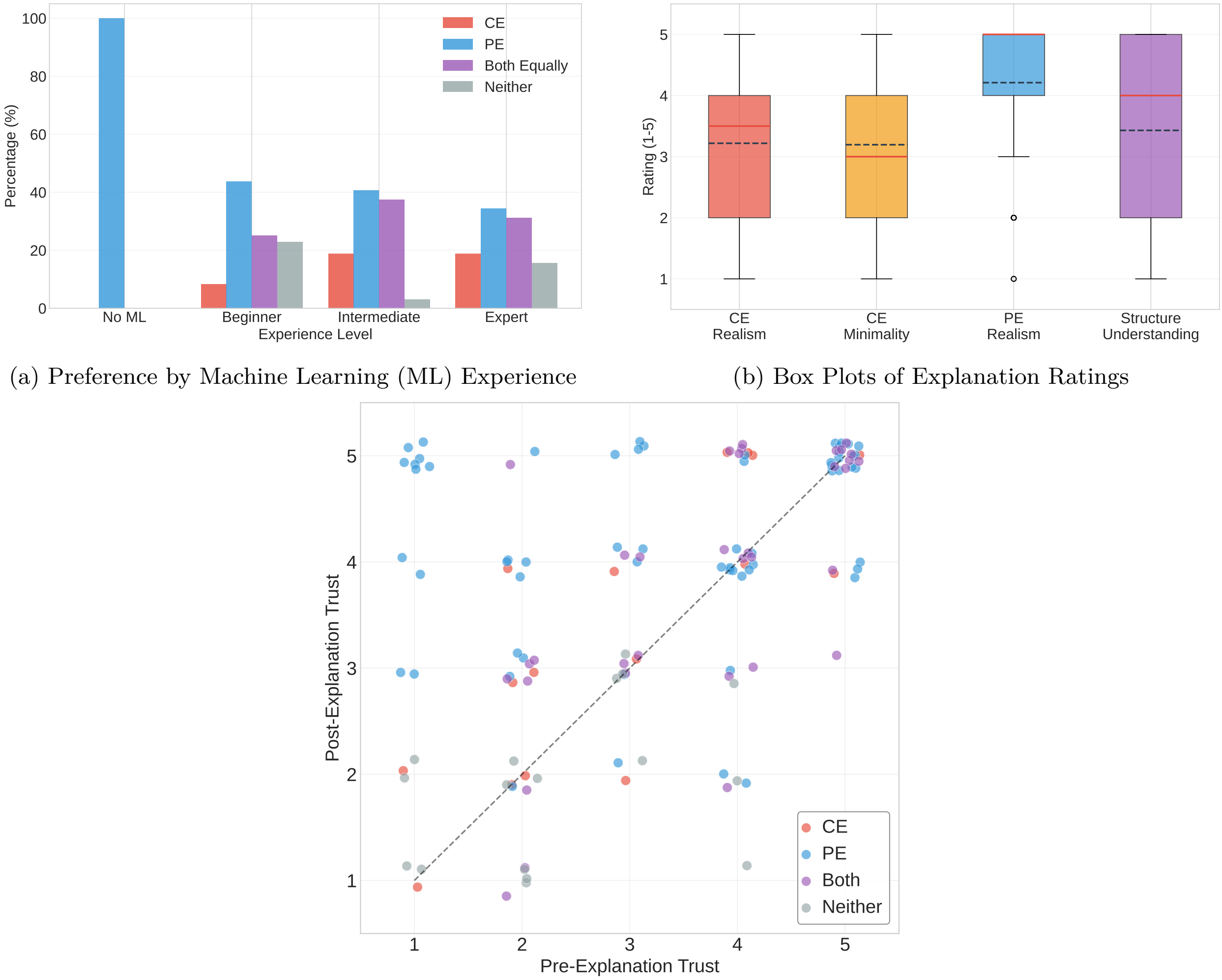

(a) Preference by Machine Learning (ML) Experience

(b) Box Plots of Explanation Ratings

(c) Pre- vs. Post-Study Trust Change

Figure 7: Summary of human evaluation results.

All ratings used a 5-point Likert scale (1 = very poor, 5 = excellent). Comparative preference was recorded using six options: Strongly CE, CE, Both Equally, PE, Strongly PE, Neither. The SE were excluded to reduce cognitive load, as they are implicitly incorporated within the CE generation pipeline.

Participants assessed explanations based on Visual Realism (the plausibility and consistency of the generated image within the SONAR distribution) and Minimality (the extent to which only necessary structural changes were introduced to the query, applicable to CE only).

The presentation order of explanations was randomised to reduce priming effects and method bias.

Figure 7 summarises the results of our user study. Overall, participants rated PEs more favourably than CE. However, the difference between PE and CE ratings decreases as participants' machine learning experience increases (Figure 7a). Box plots of the four main metrics (CE Realism, CE Minimality, PE Realism, and Structure Understanding) are shown in Figure 7b. Prototype realism is much higher than counterfactual realism, reflecting the perceptual advantage of direct sequence from RGB to SONAR representation. Structure understanding varied with participant expertise and domain knowledge, suggesting that prior familiarity with ML and visual concepts affects interpretability.

We also analysed the shift in trust ratings following exposure to the explanations. As shown in Figure 7c, the D-SCOPE framework notably tended to improve trust among participants who initially reported low confidence in the classifier's predictions. PEs were generally easier for end-users to interpret, as they operate in the RGB domain and visually illustrate the transition to the SONAR domain, whereas CEs typically require more specialised expertise and domain knowledge. These results indicate supporting evidence that perceptually realistic explanations can enhance user trust and interpretability, particularly for participants with limited prior experience.

5 Conclusions

This work introduced D-SCOPE, a post-hoc explainability framework that provides counterfactual (CE), semi-factual (SE), and prototype-based (PE) explanations for SONAR imagery. D-SCOPE does not require access to the internal structure or parameters of the classifier. Instead, it relies on class-conditional diffusion models to generate visual explanations. We evaluated it on two marine debris datasets: *Turntable* and *Watertank* (Valdenegro-Toro et al., 2025).

This approach provides the end user with a practical solution for explainability by addressing "what-if" and "even if" scenarios. CE shows how a query image would need to change to be classified as a target class, while SE captures intermediate states before the prediction flip to reveal how gradual perturbations influence the classifier's decision. Additionally, PE maps familiar optical-domain examples into the SONAR modality, allowing users to reason about predictions through cross-domain visual analogies. A user study with non-experts in the SONAR domain further confirmed that these explanations, particularly prototypes, enhance interpretability and can improve trust in the classifier's predictions.

Several challenges remain for future exploration. Extending this framework to unknown classes is difficult, as both the diffusion model and the classifiers currently require access to the training data. Future work could explore generalisation to unseen data, possibly by leveraging zero-shot approaches. Furthermore, the visual similarity metrics used in D-SCOPE have additional limitations. SSIM is highly sensitive to alignment; minor flips, rotations, or translations can significantly distort the metric. Additionally, the FID backbone network needs fine-tuning specifically for the SONAR modality for more precise evaluation.

We refer to our approach (D-SCOPE) as visual explainability, as it provides explanations by giving examples or counterfactuals of the classifier's output decision. However, not all SONAR data can be effectively interpreted through visual means alone. In several cases, particularly in the turntable dataset, certain SONAR images appear as near-random noise to the human eye, despite containing meaningful acoustic patterns. This highlights the potential need for acoustic explainability, where explanations are derived from signal-level properties rather than visual appearance. Future work could explore this direction by incorporating domain-specific acoustic attributes, such as object-specific backscatter characteristics or estimated acoustic impedance, to explain how sound interacts with underwater materials and shapes. Such an approach could complement visual explanations and provide interpretability even when visual cues are absent or ambiguous.

References

Takuya Akiba, Shotaro Sano, Toshihiko Yanase, Takeru Ohta, and Masanori Koyama. Optuna: A next-generation hyperparameter optimization framework. In *Proceedings of the 25th ACM SIGKDD international conference on knowledge discovery & data mining*, pp. 2623–2631, 2019.

Shahin Atakishiyev, Mohammad Salameh, Hengshuai Yao, and Randy Goebel. Explainable artificial intelligence for autonomous driving: A comprehensive overview and field guide for future research directions. *IEEE Access*, 2024.

Martin Atzmueller, Johannes Fürnkranz, Tomáš Kliegr, and Ute Schmid. Explainable and interpretable machine learning and data mining. *Data Mining and Knowledge Discovery*, 38(5):2571–2595, 2024. doi: 10.1007/s10618-024-01041-y.

Martin Aubard, László Antal, Ana Madureira, and Erika Ábrahám. Knowledge distillation in yolox-vit for side-scan sonar object detection. *arXiv preprint arXiv:2403.09313*, 2024.

Shahab S Band, Atefeh Yarahmadi, Chung-Chian Hsu, Meghdad Biyari, Mehdi Sookhak, Rasoul Ameri, Iman Dehzangi, Anthony Theodore Chronopoulos, and Huey-Wen Liang. Application of explainable artificial intelligence in medical health: A systematic review of interpretability methods. *Informatics in Medicine Unlocked*, 40:101286, 2023.

Chaofan Chen, Oscar Li, Daniel Tao, Alina Barnett, Cynthia Rudin, and Jonathan K Su. This looks like that: deep learning for interpretable image recognition. *Advances in neural information processing systems*, 32, 2019.

Haiyang Chen. Challenges and corresponding solutions of generative adversarial networks (gans): a survey study. In *Journal of Physics: Conference Series*, volume 1827, pp. 012066. IOP Publishing, 2021.

Florinel-Alin Croitoru, Vlad Hondru, Radu Tudor Ionescu, and Mubarak Shah. Diffusion models in vision: A survey. *IEEE Transactions on Pattern Analysis and Machine Intelligence*, 45(9):10850–10869, 2023.

Prafulla Dhariwal and Alexander Nichol. Diffusion models beat gans on image synthesis. *Advances in neural information processing systems*, 34:8780–8794, 2021.

Tarek A El-Mihoub, Abdulhakim El Gadi, Lars Nolle, and Frederic Stahl. On object detection and explainability with sonar imagery. In *2024 IEEE 4th International Maghreb Meeting of the Conference on Sciences and Techniques of Automatic Control and Computer Engineering (MI-STA)*, pp. 779–786. IEEE, 2024.

Ahmed H Elsayed, Andrej Lejman, and Frederic Stahl. Human-robot collaboration system setup for weed harvesting scenarios in aquatic lakes. *arXiv preprint arXiv:2410.17685*, 2024.

Gian Mario Favero, Parham Saremi, Emily Kaczmarek, Brennan Nichyporuk, and Tal Arbel. Conditional diffusion models are medical image classifiers that provide explainability and uncertainty for free. *arXiv preprint arXiv:2502.03687*, 2025.

Courtney Ford and Mark T Keane. Explaining classifications to non-experts: an xai user study of post-hoc explanations for a classifier when people lack expertise. In *International Conference on Pattern Recognition*, pp. 246–260. Springer, 2022.

Ian J Goodfellow, Jean Pouget-Abadie, Mehdi Mirza, Bing Xu, David Warde-Farley, Sherjil Ozair, Aaron Courville, and Yoshua Bengio. Generative adversarial nets. *Advances in neural information processing systems*, 27, 2014.

Yash Goyal, Ziyan Wu, Jan Ernst, Dhruv Batra, Devi Parikh, and Stefan Lee. Counterfactual visual explanations. In *International Conference on Machine Learning*, pp. 2376–2384. PMLR, 2019.

David Gunning, Mark Stefik, Jaesik Choi, Timothy Miller, Simone Stumpf, and Guang-Zhong Yang. Xai—explainable artificial intelligence. *Science robotics*, 4(37):eaay7120, 2019.

Martin Heusel, Hubert Ramsauer, Thomas Unterthiner, Bernhard Nessler, and Sepp Hochreiter. Gans trained by a two time-scale update rule converge to a local nash equilibrium. *Advances in neural information processing systems*, 30, 2017.

Jonathan Ho, Ajay Jain, and Pieter Abbeel. Denoising diffusion probabilistic models. *Advances in neural information processing systems*, 33:6840–6851, 2020.

Guillaume Jeanneret, Loïc Simon, and Frédéric Jurie. Diffusion models for counterfactual explanations. In *Proceedings of the Asian conference on computer vision*, pp. 858–876, 2022.

Eoin M Kenny and Mark T Keane. On generating plausible counterfactual and semi-factual explanations for deep learning. In *Proceedings of the AAAI Conference on Artificial Intelligence*, volume 35, pp. 11575–11585, 2021.

Won Jun Kim, Hyungjin Chung, Jaemin Kim, Sangmin Lee, Byeongsu Sim, and Jong Chul Ye. Derivative-free diffusion manifold-constrained gradient for unified xai. *arXiv preprint arXiv:2411.15265*, 2024.

Tuomas Kynkäänniemi, Tero Karras, Samuli Laine, Jaakko Lehtinen, and Timo Aila. Improved precision and recall metric for assessing generative models. *Advances in neural information processing systems*, 32, 2019.

Jun Li, Chenyang Zhang, Wei Zhu, and Yawei Ren. A comprehensive survey of image generation models based on deep learning. *Annals of Data Science*, 12(1):141–170, 2025.

Oscar Li, Hao Liu, Chaofan Chen, and Cynthia Rudin. Deep learning for case-based reasoning through prototypes: A neural network that explains its predictions. In *Proceedings of the AAAI conference on artificial intelligence*, volume 32, 2018.

Zikang Li, Zhuojun Xie, Puhong Duan, Xudong Kang, and Shutao Li. Dual spatial attention network for underwater object detection with sonar imagery. *IEEE Sensors Journal*, 24(5):6998–7008, 2024.

Scott M Lundberg and Su-In Lee. A unified approach to interpreting model predictions. *Advances in neural information processing systems*, 30, 2017.

C. Manss and T. A. El-Mihoub. Evaluation of explanations for object detection using transformers with sonar data. In *Artificial Intelligence XL*, Chambridge, 2025. Springer Nature Switzerland.

Silvan Mertes, Tobias Huber, Katharina Weitz, Alexander Heimerl, and Elisabeth André. Ganterfactual—counterfactual explanations for medical non-experts using generative adversarial learning. *Frontiers in artificial intelligence*, 5:825565, 2022.

Purushothaman Natarajan and Athira Nambiar. Underwater sonar image classification and analysis using lime-based explainable artificial intelligence. *arXiv preprint arXiv:2408.12837*, 2024.

Meike Nauta, Annemarie Jutte, Jesper Provoost, and Christin Seifert. This looks like that, because... explaining prototypes for interpretable image recognition. In *Joint European Conference on Machine Learning and Knowledge Discovery in Databases*, pp. 441–456. Springer, 2021.

Alexander Quinn Nichol and Prafulla Dhariwal. Improved denoising diffusion probabilistic models. In *International conference on machine learning*, pp. 8162–8171. PMLR, 2021.

Lars Nolle, Frederic Stahl, and Tarek El-Mihoub. On explanations for hybrid artificial intelligence. In *International Conference on Innovative Techniques and Applications of Artificial Intelligence*, pp. 3–15. Springer, 2023.

Stephen M Pizer, E Philip Amburn, John D Austin, Robert Cromartie, Ari Geselowitz, Trey Greer, Bart ter Haar Romeny, John B Zimmerman, and Karel Zuiderveld. Adaptive histogram equalization and its variations. *Computer vision, graphics, and image processing*, 39(3):355–368, 1987.

Marco Tulio Ribeiro, Sameer Singh, and Carlos Guestrin. " why should i trust you?" explaining the predictions of any classifier. In *Proceedings of the 22nd ACM SIGKDD international conference on knowledge discovery and data mining*, pp. 1135–1144, 2016.

Guy-Junior Richard, Jérôme Habonneau, Didier Guériot, and Jean-Marc Le Caillec. Ai explainability and acceptance: A case study for underwater mine hunting. *ACM Journal of Data and Information Quality*, 16(1):1–20, 2024.

Dawid Rymarczyk, Łukasz Struski, Michał Górszczak, Koryna Lewandowska, Jacek Tabor, and Bartosz Zieliński. Interpretable image classification with differentiable prototypes assignment. In *European Conference on Computer Vision*, pp. 351–368. Springer, 2022.

Chitwan Saharia, William Chan, Huiwen Chang, Chris Lee, Jonathan Ho, Tim Salimans, David Fleet, and Mohammad Norouzi. Palette: Image-to-image diffusion models. In *ACM SIGGRAPH 2022 conference proceedings*, pp. 1–10, 2022.

Philipp Schlinge, Steffen Meinert, and Martin Atzmueller. Comprehensive evaluation of prototype neural networks. *KI-Künstliche Intelligenz*, pp. 1–20, 2025.

Deepak Singh and Matias Valdenegro-Toro. The marine debris dataset for forward-looking sonar semantic segmentation. In *Proceedings of the ieee/cvf international conference on computer vision*, pp. 3741–3749, 2021.

Jascha Sohl-Dickstein, Eric Weiss, Niru Maheswaranathan, and Surya Ganguli. Deep unsupervised learning using nonequilibrium thermodynamics. In *International conference on machine learning*, pp. 2256–2265. pmlr, 2015.

Matias Valdenegro-Toro, Deepan Chakravarthi Padmanabhan, Deepak Singh, Bilal Wehbe, and Yvan Petillot. The marine debris forward-looking sonar datasets. *arXiv preprint arXiv:2503.22880*, 2025.

Arnaud Van Looveren, Janis Klaise, Giovanni Vacanti, and Oliver Cobb. Conditional generative models for counterfactual explanations. *arXiv preprint arXiv:2101.10123*, 2021.

Payal Varshney, Adriano Lucieri, Christoph Balada, Andreas Dengel, and Sheraz Ahmed. Generating counterfactual trajectories with latent diffusion models for concept discovery. In *International Conference on Pattern Recognition*, pp. 138–153. Springer, 2025.

Sahil Verma, John Dickerson, and Keegan Hines. Counterfactual explanations for machine learning: A review. *arXiv preprint arXiv:2010.10596*, 2(1):1, 2020.

Sandra Wachter, Brent Mittelstadt, and Chris Russell. Counterfactual explanations without opening the black box: Automated decisions and the gdpr. *Harv. JL & Tech.*, 31:841, 2017.

Sarah Walker, Joshua Peeples, Jeff Dale, James Keller, and Alina Zare. Explainable systematic analysis for synthetic aperture sonar imagery. In *2021 IEEE International Geoscience and Remote Sensing Symposium IGARSS*, pp. 2835–2838. IEEE, 2021.

Zhou Wang, Alan C Bovik, Hamid R Sheikh, and Eero P Simoncelli. Image quality assessment: from error visibility to structural similarity. *IEEE transactions on image processing*, 13(4):600–612, 2004.

Bilal Wehbe, Nimish Shah, Miguel Bande, and Christian Backe. Sonar-to-rgb image translation for diver monitoring in poor visibility environments. In *OCEANS 2022, Hampton Roads*, pp. 1–9. IEEE, 2022.

Xin Wen, Feihu Zhang, Chensheng Cheng, Xujia Hou, and yGuang Pan. Side-scan sonar underwater target detection: Combining the diffusion model with an improved yolov7 model. *IEEE Journal of Oceanic Engineering*, 2024.

Ling Yang, Zhilong Zhang, Yang Song, Shenda Hong, Runsheng Xu, Yue Zhao, Wentao Zhang, Bin Cui, and Ming-Hsuan Yang. Diffusion models: A comprehensive survey of methods and applications. *ACM Computing Surveys*, 56(4):1–39, 2023.

Matei Zaharia, Andrew Chen, Aaron Davidson, Ali Ghodsi, Sue Ann Hong, Andy Konwinski, Siddharth Murching, Tomas Nykodym, Paul Ogilvie, Mani Parkhe, et al. Accelerating the machine learning lifecycle with mlflow. *IEEE Data Eng. Bull.*, 41(4):39–45, 2018.

Mehdi Zemni, Mickaël Chen, Éloi Zablocki, Hédi Ben-Younes, Patrick Pérez, and Matthieu Cord. Octet: Object-aware counterfactual explanations. In *Proceedings of the IEEE/CVF conference on computer vision and pattern recognition*, pp. 15062–15071, 2023.

Haoting Zhang, Mei Tian, Gaoping Shao, Juan Cheng, and Jingjing Liu. Target detection of forward-looking sonar image based on improved yolov5. *IEEE Access*, 10:18023–18034, 2022.

Lvmin Zhang, Anyi Rao, and Maneesh Agrawala. Adding conditional control to text-to-image diffusion models. In *Proceedings of the IEEE/CVF international conference on computer vision*, pp. 3836–3847, 2023.